

Counterfactual Generative Models for Time-Varying Treatments

Shenghao Wu¹, Wenbin Zhou¹, Minshuo Chen², and Shixiang Zhu¹

¹ Carnegie Mellon University

² Princeton University

May 26, 2023

Abstract

Estimating average causal effects is a common practice to test new treatments. However, the average effect “masks” important individual characteristics in the counterfactual distribution, which may lead to safety, fairness and ethical concerns. This issue is exacerbated in the temporal setting, where the treatment is sequential and time-varying, leading to an intricate influence on the counterfactual distribution. In this paper, we propose a novel conditional generative modeling approach to capture the whole counterfactual distribution, allowing efficient inference on certain statistics of the counterfactual distribution. This makes the proposed approach particularly suitable for healthcare and public policy making. Our generative modeling approach carefully tackles the distribution mismatch in the observed data and the targeted counterfactual distribution via a marginal structural model. Our method outperforms state-of-the-art baselines on both synthetic and real data.

1 Introduction

Estimating time-varying treatment effects from observational data has garnered significant attention due to the growing prevalence of time-series records. One field where this is especially relevant is public health policy [27, 66], particularly in making decisions related to interventions during pandemics, such as implementing mask mandates to control the spread of the virus. These interventions are implemented at different points in time and can have varying effects over time. The ability to accurately estimate such effects provides policymakers and researchers with valuable insights into the policy’s impact on the development of future infectious cases in a timely manner. This is essential for evaluating the effectiveness of the policy and making informed decisions about its continuation or modification.

Most of the existing research primarily focuses on measuring the effects of treatments by looking at the average outcomes [17, 21, 49]. This is a sensible approach to test how effective new treatments are for the entire population. However, this approach may overlook significant differences in the distributions of counterfactual outcomes beyond a simple shift in the average, especially when the underlying distribution of causal effects is heterogeneous. More importantly, the impact of a time-dependent treatment can accumulate or grow over time, leading to a larger distributional discrepancy between observed and counterfactual outcomes, as shown in Figure 1. As a result, it becomes more challenging to obtain a comprehensive understanding of the range of possible outcomes due to the extensive array of treatment options and the limited availability of data on different treatment combinations. In the context of a mask mandate for COVID-19, such accumulative effects can be observed as individuals gradually

* Heterogeneous effect

* Distributional discrepancy between observed and counterfactual outcomes

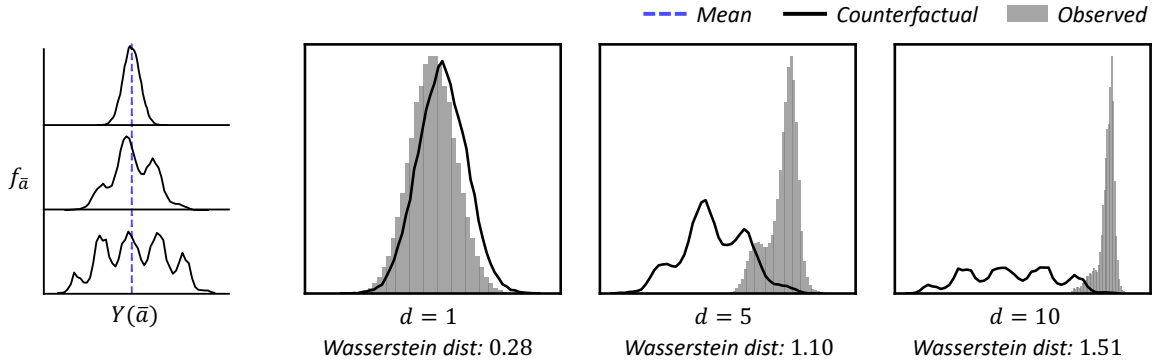


Figure 1: An illustrative example of the counterfactual distribution of an outcome variable given a time-varying treatments, with different lengths of treatment history. The panel on the left shows that the mean is incapable of describing the heterogeneous effect in counterfactual distributions. The rest of three panels demonstrates how the length of the treatment history affects the distribution. Here d denotes the length of the history dependence. The longer the dependence on the treatment history, the greater the distributional mismatch tends to be.

adopt mask-wearing behaviors and adhere to the mandate more strictly over time. Initially, the impact of the mask mandate may be limited as people adapt to the new requirement. However, as compliance increases and more individuals wear masks consistently, the accumulative effects can become more pronounced, resulting in a larger reduction in COVID-19 cases.

To tackle this challenge, we propose a novel framework that can simulate all possible counterfactual outcomes under a time-varying treatment. Our approach aims to estimate the complete counterfactual distribution, going beyond a narrow focus on specific statistics such as the mean. In particular, instead of explicitly defining the outcome using a parametric model, our objective is to develop a conditional generator [34, 57]. This generator, which we choose in a flexible manner, takes into account the treatment history as input and generates realistic counterfactual outcomes that align with the underlying distribution of counterfactuals. The key idea behind our framework is to utilize a “proxy” conditional distribution as an approximation of the true counterfactual distribution. To achieve this, we establish a statistical relationship between the observed and counterfactual distributions inspired by g-formula [9, 37, 45, 51]. Then the optimal conditional generator can be found by minimizing the Kullback-Leibler (KL) divergence between the re-weighted observed distribution, which is obtained through a marginal structural model (MSM), and the proxy conditional distribution represented by the generator. We extensively evaluate our framework through numerical experiments on synthetic and real-world data sets. The results validate that the generated outcomes closely approximate the true counterfactual distribution across diverse scenarios, surpassing state-of-the-art baselines. In summary, our approach offers the following major contributions:

1. We bridge the gap between causal inference and conditional generative modeling by following the idea of g-formula. This approach allows us to effectively address the distributional mismatch under the time-series setting, providing a streamlined solution.
2. Thanks to the generative nature of our model, we can obtain a complete assessment of time-varying treatment effects by generating potential outcomes from the underlying counterfactual distribution.

3. As we do not impose constraints on the generator’s form, our proposed framework possesses substantial representational power, enabling it to capture complex structures in the effects of time-varying treatments, which has been validated by both synthetic and real results.
4. Our framework is versatile and model-agnostic, allowing causal analysis to leverage a wide range of generative models and cutting-edge learning algorithms.

1.1 Related work

Our work has connections to causal inference in time series, counterfactual distribution estimation, and generative models. To our best knowledge, our work is the first to intersect the three aforementioned areas. Below we review each of these areas independently.

Causal inference with time-varying treatments Causal inference has historically been related to longitudinal data. Classic approaches to analyzing time-varying treatment effects include the g-computation formula, structural nested models, and marginal structural models [9, 43, 44, 47, 48, 51]. These seminal works are typically based on parametric models with limited flexibility. Recent advancements in machine learning have significantly accelerated progress in this area using flexible statistical models [6, 54] and deep neural networks [4, 29, 55] to capture the complex temporal dependency of the outcome on treatment and covariate history. These approaches, however, focus on predicting the mean counterfactual outcome instead of the distribution. The performance of these methods also heavily relies on the specific types of models (*e.g.*, LSTMs) without a framework generalizable to other models.

Counterfactual distribution estimation Recently, several approaches have emerged to estimate the entire counterfactual distribution rather than the means, including estimating quantiles of the cumulative distributional functions (CDFs) [7, 62], re-weighted kernel estimations [8], and semiparametric methods [22]. In particular, [22] highlights the extra information afforded by estimating the entire counterfactual distribution and using the distance between counterfactual densities as a measure of causal effects. However, these methods are designed to work under static settings with no time-varying treatments and inherently falls under the standard supervised learning scheme, lacking the capability to extrapolate under unbalanced or even unobserved counterfactual settings [2]. Our work, on the other hand, aims to approximate the counterfactual distribution using generative models, enabling a wider range of application scenarios including continuous treatments and can accommodate more intricate data structures.

Counterfactual generative model Generative models, including a variety of deep network architectures such as generative adversarial networks (GAN) and autoencoders, have been recently developed to estimate counterfactual outcomes [3, 12, 14, 19, 28, 31, 32, 42, 52, 53, 61, 65, 67]. However, many of these approaches primarily focus on learning causal latent representations to improve counterfactual estimation accuracy rather than obtaining the distribution of the counterfactual outcome. For example, [52, 65] adopt deep generative models to improve the estimation of individual treatment effects (ITEs) under static settings. Some of these approaches focus on generating a realistic counterfactual sample (such as a “what-if” image) instead of quantifying the counterfactual distributions [42, 53, 61]. Furthermore, there has been limited exploration of applying generative models to time series settings in the existing literature. A few attempts, including [28, 32], train autoencoders to estimate treatment effect using longitudinal data. Nevertheless, these methods are not intended for obtaining counterfactual distributions. In sum, to the best of our knowledge, our work is the first to use

generative models to learn counterfactual distribution from data with time-varying treatments, a novel setting not addressed by prior works.

2 Methodology

2.1 Problem setup

In this study, we consider the treatment for each discrete time period (such as day or week) as a random variable $A_t \in \mathcal{A}$, where $t = 1, \dots, T$ and T is the total number of time periods. We let $X_t \in \mathcal{X}$ be the set of possibly time-varying covariates that are realized prior to A_t but after A_{t-1} . The subject’s outcome $Y_t \in \mathcal{Y}$ at time t depends on its previous treatment history from time $t - d + 1$ to t , denoted as $\bar{A}_t = \{A_{t-d+1}, \dots, A_t\}$, where d is the length of history dependence. The possible change in treatment at time t occurs after data are available on the covariate history $\bar{X}_t = \{X_{t-d+1}, \dots, X_t\}$. In the above notation, lowercase letters refer to the possible values of a random variable. We use y_t , a_t , and x_t to represent a realization of Y_t , A_t , and X_t , respectively. We also use $\bar{a}_t = (a_{t-d+1}, \dots, a_t)$ and $\bar{x}_t = (x_{t-d+1}, \dots, x_t)$ to denote the history of treatment and covariate realizations. For the sake of simplicity, we omit the subscript t going forward and use Y , \bar{A} , and \bar{X} as shorthand for Y_t , \bar{A}_t , and \bar{X}_t in the rest of the paper.

The goal of our study is to analyze the effect of a time-varying treatment \bar{A} on the outcome Y and learn its counterfactual distribution using observed data. Specifically, we let $Y(\bar{a})$ denote the counterfactual or potential outcome for a subject under a time-varying treatment \bar{a} , and define $f_{\bar{a}}$ as the underlying distribution of $Y(\bar{a})$. We note that $f_{\bar{a}}$ is different from the marginal density of Y , as the treatment is fixed at $\bar{A} = \bar{a}$ in the conditioning. It is also not equal to the unadjusted conditional density $f(y|\bar{a})$. Instead, $f_{\bar{a}}$ is the density of the counterfactual variable $Y(\bar{a})$, which represents the outcome that would have been observed if treatment were set to $\bar{A} = \bar{a}$, if the standard assumptions [47, 29] hold. See Appendix A for more details about assumptions.

2.2 Counterfactual generative framework for time-varying treatments

This paper proposes a counterfactual generator, denoted as g_θ , to simulate $Y(\bar{a})$ according to the *proxy conditional distribution* $f_\theta(y|\bar{a})$ instead of directly modeling its expectation or specifying a parametric counterfactual distribution. Here we use $\theta \in \Theta$ to represent the model’s parameters, and formally define the generator as a function:

$$g_\theta(z, \bar{a}) : \mathbb{R}^r \times \mathcal{A}^d \rightarrow \mathcal{Y}. \quad (1)$$

The generator takes as input a random noise vector ($z \in \mathbb{R}^r \sim \mathcal{N}(0, I)$) and the time-varying treatment \bar{a} . The output of the generator is a sample of possible counterfactual outcomes that follows the proxy conditional distribution represented by θ , *i.e.*,

$$y \sim f_\theta(\cdot|\bar{a}),$$

which can be viewed as an approximate of the underlying counterfactual distribution $f_{\bar{a}}$. Figure 2 shows an overview of the proposed generative model architecture.

Marginal structural generative models The learning objective is to find the optimal generator that minimizes the distance between the proxy conditional distribution $f_\theta(\cdot|\bar{a})$ and the true counterfactual distribution $f_{\bar{a}}$, as illustrated in Figure 3. If the distance metric is

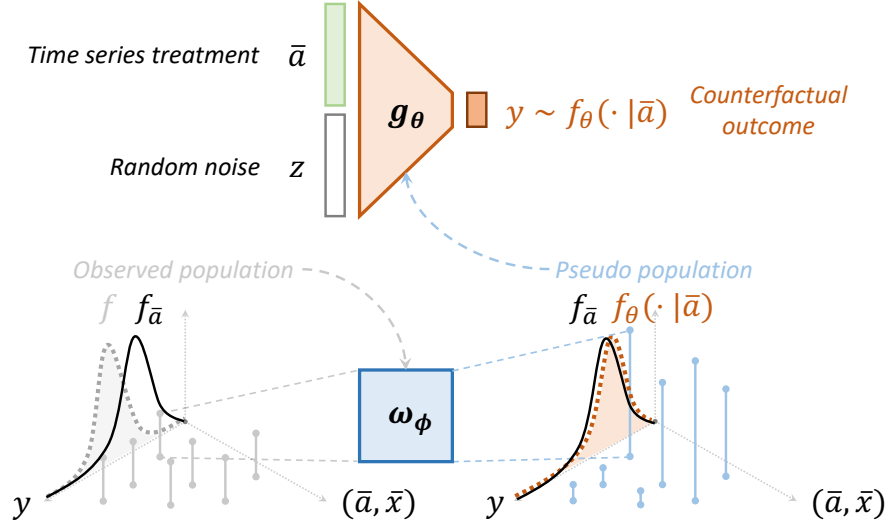


Figure 2: The architecture of the proposed counterfactual generative models. The generator g_θ is designed to produce samples of the outcome variable $Y(\bar{a})$ with a given time-varying treatment \bar{a} . The generated samples are expected to conform to the proxy conditional distribution f_θ , which is an approximate of the underlying counterfactual distribution $f_{\bar{a}}$. The generator is trained using a pseudo population created by reweighting each data tuple according to its IPTW w_ϕ . The IPTW can be estimated from the observed data.

Kullback-Leibler (KL) divergence, this objective can be expressed equivalently by maximizing the log-likelihood [36]:

$$\max_{\theta \in \Theta} \ell(\theta) := \mathbb{E}_{y \sim f_{\bar{a}}} \log f_\theta(y|\bar{a}), \quad (2)$$

To obtain samples from the counterfactual distribution $f_{\bar{a}}$, we follow the idea of marginal structural models (MSMs) introduced by [37, 51, 45] and extended by [9] to account for time-varying treatments. Specifically, we introduce Lemma 1, which establishes a connection between the counterfactual distribution and the data distribution. The proof of the Lemma is provided in Appendix B.

Lemma 1. *Under unconfoundedness and positivity, we have*

$$f_{\bar{a}}(y) = \int \frac{\mathbb{1}\{\bar{A} = \bar{a}\}}{\prod_{\tau=t-d}^t f(A_\tau | \bar{A}_{\tau-1}, \bar{X}_\tau)} f(y, \bar{A}, \bar{X}) d\bar{A}d\bar{X}, \quad (3)$$

where f denotes the observed data distribution.

Now we present a proposition using Lemma 1, allowing us to substitute the expectation in (2), computed over a counterfactual distribution, with the sample average over a pseudo-population. This pseudo-population is constructed by assigning weights to each data tuple based on their subject-specific *inverse probability of treatment weight* (IPTW). See the proof in Appendix C.

Proposition 1. *Let \mathcal{D} denote the set of observed data tuples. The generative learning objective can be approximated by:*

$$\mathbb{E}_{y \sim f_{\bar{a}}} \log f_\theta(y|\bar{a}) \approx \sum_{(y, \bar{a}, \bar{x}) \in \mathcal{D}} w_\phi(\bar{a}, \bar{x}) \log f_\theta(y|\bar{a}), \quad (4)$$

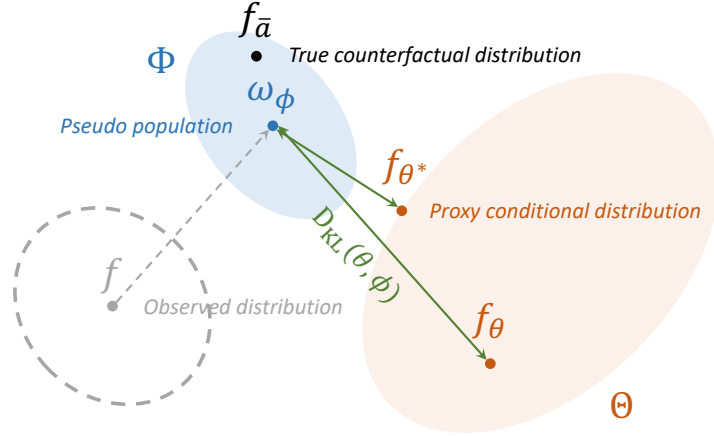


Figure 3: An illustration of our learning objective. We aim to minimize the KL-divergence between the proxy conditional distribution $f_{\theta}(\cdot|\bar{a})$ and the true counterfactual distribution $f_{\bar{a}}$. Because $f_{\bar{a}}$ is not directly accessible, we obtain samples from a pseudo population created by another model ϕ . Here θ^* denotes the optimal generator that minimizes the KL-divergence between $f_{\theta}(\cdot|\bar{a})$ and the pseudo population.

where $w_{\phi}(\bar{a}, \bar{x})$ denotes the subject-specific IPTW, parameterized by $\phi \in \Phi$, which takes the form:

$$w_{\phi}(\bar{a}, \bar{x}) = \frac{1}{\prod_{\tau=t-d}^t f_{\phi}(a_{\tau}|\bar{a}_{\tau-1}, \bar{x}_{\tau})}. \quad (5)$$

Here we use another model, denoted by $\phi \in \Phi$, to represent the conditional probability $f(A_{\tau}|\bar{A}_{\tau}, \bar{X}_{\tau})$, which defines the IPTW w_{ϕ} and can be learned separately using observed data. Note that the effectiveness of this method is dependent on a correct specification of the IPTW ϕ (i.e., the black dot is inside of the blue area in Figure 3) [9, 29]. In [29], they use an RNN-like structure to represent the conditional probability f_{ϕ} without making strong assumptions on the form of the conditional probability. The choice of g_{θ} and f_{ϕ} are entirely general and both can be specified using deep architectures. In this paper, we use fully-connected neural networks for both g_{θ} and f_{ϕ} .

Algorithm 1 Learning algorithm for the conditional generator θ

Input: Training set \mathcal{D} data tuples: $\mathcal{D} = \{(y_t^{(i)}, \bar{a}_t^{(i)}, \bar{x}_t^{(i)})\}_{t=d, \dots, T, i=1, \dots, N}$ where T is the time horizon and I is the total number of individuals; the number of the learning epoches E .

Initialization: model parameters θ and fitted $\hat{\phi}$ using \mathcal{D} .

while $e < E$ **do**

for each sampled batch \mathcal{D}^k with size n **do**

1. Draw samples $\epsilon \sim \mathcal{N}(0, I)$ from noise distribution;
2. Compute the ELBO of $\log f_{\theta}(y|\bar{a})$ for $(y, \bar{a}, \bar{x}) \in \mathcal{D}^k$ given ϵ and θ according to (6);
3. Re-weight the ELBO for $(y, \bar{a}, \bar{x}) \in \mathcal{D}^k$ using $w_{\hat{\phi}}(\bar{a}, \bar{x})$ according to (5);
4. Update θ using stochastic gradient descent by maximizing (4).

end for

end while

return θ

Variational approximation and learning To compute the weighted log-likelihood as expressed in (4) and learn the proposed generative model, we use a variational method. This approach is widely-adopted for learning generative models, including variational autoencoders [25, 26] and diffusion models [18, 23, 56]. In this paper, we adopt the conditional variational autoencoder (CVAE) [57] and approximate the logarithm of the proxy conditional probability using its evidence lower bound (ELBO):

$$\log f_{\theta}(y|\bar{a}) \geq -D_{\text{KL}}(q(z|y, \bar{a})||p_{\theta}(z|\bar{a})) + \mathbb{E}_{q(z|y, \bar{a})} [\log p_{\theta}(y|z, \bar{a})], \quad (6)$$

where q is a variational approximation of the posterior distribution over the random noise given observed outcome y and its treatment \bar{a} . The first term on the right-hand side is the Kullback–Leibler (KL) divergence of the approximate posterior $q(\cdot|y, \bar{a})$ from the exact posterior $p_{\theta}(\cdot|\bar{a})$. The second term is the log-likelihood of the latent data generating process.

In practice, we introduce two additional generators, including the encoder net $g_{\text{encode}}(\epsilon, y, \bar{a})$ and the prior net $g_{\text{prior}}(\epsilon, \bar{a})$, respectively, to represent $q(z|y, \bar{a})$ and $p_{\theta}(z|\bar{a})$ as transformations of another random variable $\epsilon \sim \mathcal{N}(0, I)$ using reparameterization trick [56]. Both $q(z|y, \bar{a})$ and $p_{\theta}(z|\bar{a})$ are often modeled as Gaussian distributions, which allows us to compute the KL divergence of Gaussians with a closed-form expression. The log-likelihood of the second term can be implemented as the reconstruction loss and calculated using generated samples. We summarize our learning procedure in Algorithm 1. The complete derivation of (6) and implementation details can be found in Appendix D.

3 Experiments

We test our method using numerical examples and demonstrate the superior performance compared to four state-of-the-art methods, including (1) Conditional Variational Autoencoder (CVAE) [57], (2) Marginal structural model (MSM) [46], (3) Kernel Density Estimation (KDE)[50] and (4) Kernel Density Estimation based on pseudo-population (IPTW+KDE). See Appendix E.1 for a detailed review of these baseline methods. In the following, we refer to our proposed conditional event generator as marginal structural conditional variational autoencoder (MSCVAE).

Experiment set-up We use the same fully-connected neural network architecture to represent the counterfactual generator g_{θ} , the IPTW w_{ϕ} , and the encoder network g_{encode} . This network has two hidden layers, each consisting of 1,000 units and employs the Rectified Linear Unit (ReLU) activation function. We add an additional Sigmoid layer to the network of the IPTW, since we consider a dichotomous treatment variable $A_t \in \{0, 1\}$ in our experiments. To learn the model parameter θ , we use stochastic gradient descent to maximize the weighted log-likelihood (4). We adopt an Adam optimizer [24] with a learning rate of 10^{-3} and a batch size of 256. To ensure learning stability, we follow a commonly-used practice [64, 29] that involves truncating the subject-specific IPTW weights at the 0.01-th and 99.99-th percentiles and normalizing them by their mean. All experiments are performed on Jupyter Notebook with 16GB RAM and a 2.6 GHz 6-Core Intel Core i7 CPU. More details of the experiment set-up can be found in Appendix E.2.

3.1 Synthetic results

We assess the effectiveness of the proposed framework using synthetic experiments. Following the well-established methodology described in [46], we simulate three synthetic data sets with different lengths of history dependence ($d = 1, 3, 5$) using linear models. Each data set comprises 10,000 trajectories, representing recorded observations of individual subjects. These trajectories

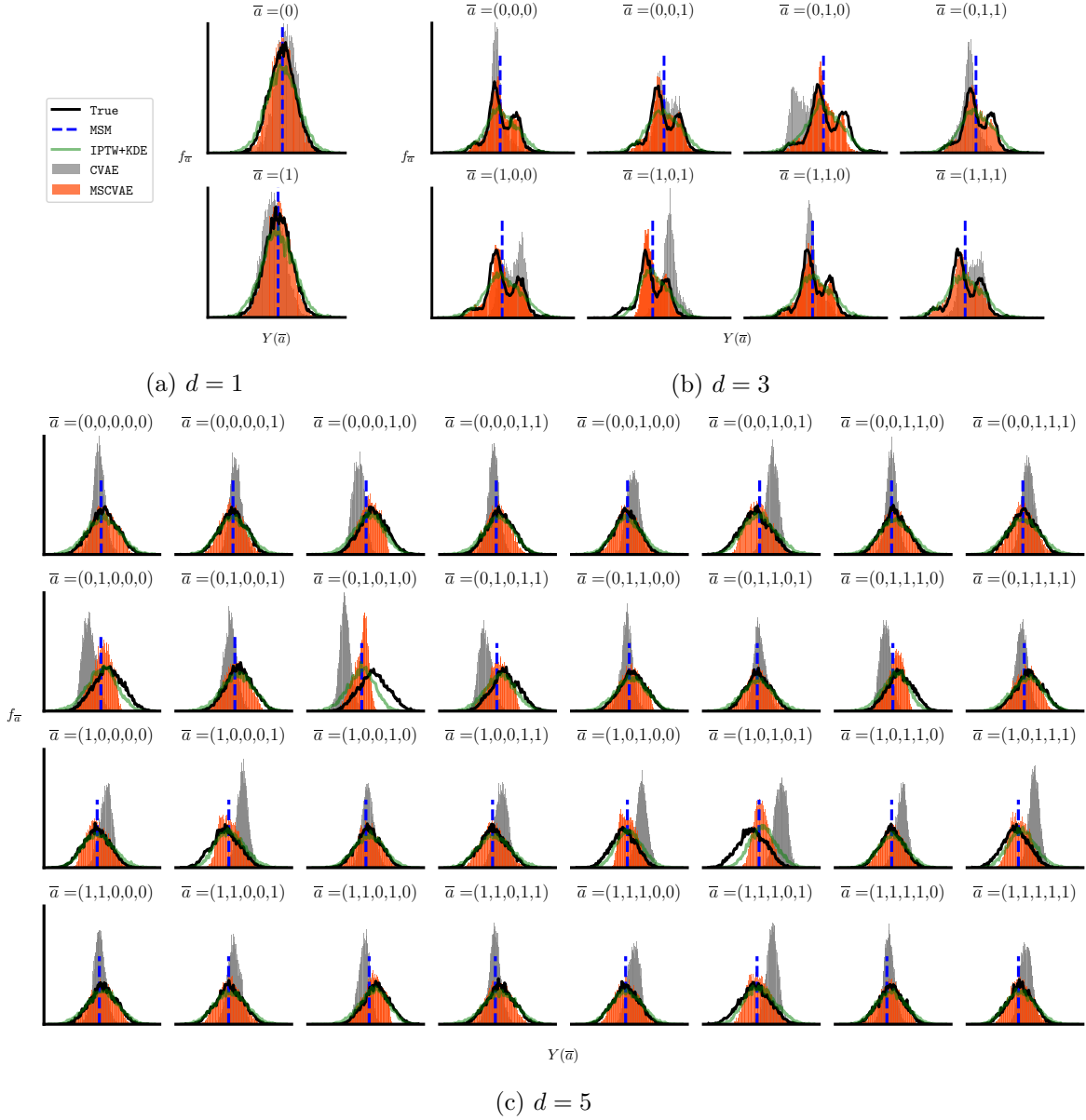


Figure 4: The estimated and true counterfactual distributions across various lengths of history dependence ($d = 1, 3, 5$) on synthetic data sets. Each sub-panel provides a comparison for a specific treatment combination \bar{a} .

consist of 100 data tuples, encompassing treatment, covariate, and outcome values at specific time points. The causal dependence between these variables is visualized in Figure 6 (Appendix B). Furthermore, we regulate the distribution of various treatment combinations in the synthetic data by manipulating the treatment intercept denoted by β_0 . Decreasing the value of β_0 leads to increased imbalances in the proportions of different treatment combinations. The primary evaluation metric involves comparing the similarity (*e.g.*, Wasserstein distance) between the estimated and true counterfactual distributions. To obtain the true counterfactual distribution, we fix the treatment in each time-varying trajectory to \bar{a} and generate the corresponding covariates and outcome using the same data generation process. See Appendix E.3 for a detailed description of the synthetic data generation.

In Figure 4, we can see visual comparisons of the true counterfactual distribution and the

Table 1: Quantitative performance of estimating counterfactual distributions on synthetic data

Methods	$\beta_0 = -0.5$ (balanced)						$\beta_0 = -2$ (imbalanced)					
	$d = 1$		$d = 3$		$d = 5$		$d = 1$		$d = 3$		$d = 5$	
	Mean	Wasserstein	Mean	Wasserstein	Mean	Wasserstein	Mean	Wasserstein	Mean	Wasserstein	Mean	Wasserstein
MSM	0.003	NA	0.055	NA	0.186	NA	0.026	NA	0.036	NA	0.132	NA
KDE	0.246	0.433	0.528	0.579	0.536	0.601	0.257	0.459	0.538	0.661	0.19	0.641
IPTW+KDE	0.010	0.127	0.048	0.133	0.146	0.181	0.010	0.122	0.068	0.217	0.157	0.213
CVAE	0.263	0.264	0.524	0.559	0.537	0.612	0.246	0.263	0.545	0.607	0.520	0.563
MSCVAE	0.008	0.053	0.043	0.107	0.147	0.171	0.006	0.065	0.064	0.175	0.161	0.186

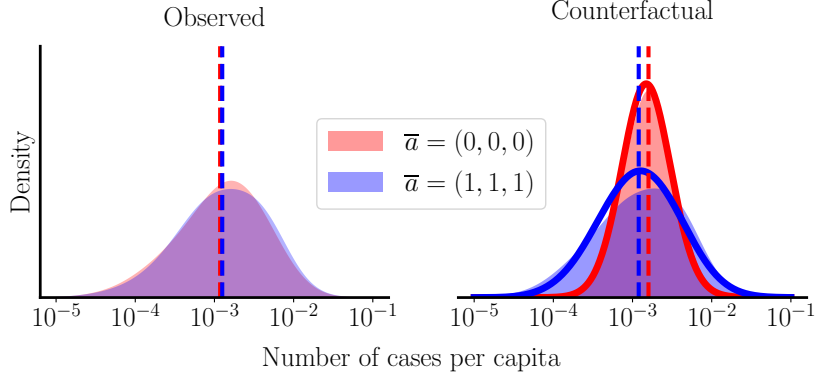


Figure 5: Observed distribution and estimated counterfactual distribution of the number of COVID-19 cases per capita under two mask policies. The solid lines and shadings represent the estimated weighted distribution using IPTW and the learned distribution using MSCVAE, respectively. The vertical dashed lines represent the mean of the corresponding distributions.

learned counterfactual distributions achieved with the proposed method. The results clearly demonstrate the superior performance of the MSCVAE (orange shading) over the baseline methods in accurately capturing the shape of the true counterfactual distributions (represented by the black line) across all scenarios. It is worth mentioning that the learned distribution produced by the CVAE using the unweighted objective function deviates significantly from the desired target and fails to accurately represent the counterfactual distributions. This emphasizes the significance of the proposed weighting scheme in achieving more precise and reliable results. For ease of the presentation, we only include results when $d = 1, 3, 5$ and $\beta_0 = -0.5$ (corresponding to a more balanced treatment distribution).

Table 1 summarizes more quantitative comparisons between MSCVAE and baseline methods. We adopt two metrics: mean distance and Wasserstein distance [11, 40, 59], to measure the discrepancies between the estimated and true counterfactual distributions. We note that the MSM is correctly specified and can only be evaluated by the mean distance as these methods are incapable of learning distributional information. From our observations, it is evident that the MSCVAE not only consistently achieves the smallest Wasserstein distance in the majority of the experimental settings, but also demonstrates highly competitive mean distances when compared to the MSM method, which is consistent with the result in Figure. 4.

3.2 Real results

We conduct experiments using real data to examine the proposed method and derive insightful policy implications based on the estimated counterfactual outcomes. Specifically, we focus on evaluating the effectiveness of mask mandates in the United States during the COVID-19 pandemic. To this end, we collected data from multiple sources, including the Centers for Disease Control and Prevention (CDC), the US Census Bureau, and a Facebook survey

[5, 10, 13, 15, 68, 69]. The data set encompasses various variables aggregated on a weekly basis at the county level. These variables include the number of cases per capita, the number of deaths per capita, the mask mandate policy (with values of 0 indicating no mandate and 1 indicating a mandate), average retail and recreation mobility, and surveyed COVID-19 symptoms. The data set covers 3,219 counties in the United States and spans 49 weeks from 2020 to 2021. In our analysis, we treat the number of cases per capita as the treatment variable, the mask mandate policy as the outcome variable, and the remaining variables as covariates within our model. To capture a relevant time window for analysis, we set the history dependence length d to 3, as most COVID-19 symptoms tend to subside within this timeframe [33]. The full description of the data set can be found in Appendix E.4.

Figure 5 illustrates a comparative analysis of the per capita distribution of new cases under two different scenarios: one without a mask mandate ($\bar{a} = (0, 0, 0)$) and the other with a full mask mandate ($\bar{a} = (1, 1, 1)$). In the left panel, we observe that the distributions under both policies appear remarkably similar, suggesting that the mask mandate has a limited impact on controlling the spread of the virus. This unexpected outcome challenges commonly held assumptions. In the right panel, we present counterfactual distributions estimated using our method, revealing a noticeable disparity between the mask mandate and no mask mandate scenarios. The mean of the distribution for mask mandate is significantly lower than that of no mask mandate. These findings indicate that implementing a mask mandate consistently for three consecutive weeks can effectively reduce the number of future new cases. It aligns with the understanding supported by health experts’ suggestions and various studies [1, 16, 38, 60, 63] regarding the effectiveness of wearing masks. Finally, it is important to note that the implementation of full mask mandates exhibits a significantly higher variance compared to the absence of a mask mandate. This implies that the impact of a mask mandate varies across different data points, specifically counties in our study. This insight highlights the need for policymakers to carefully assess the unique characteristics of their respective regions when considering the implementation of mask mandate policies. It is crucial for policymakers to understand that the effectiveness of a mask mandate may yield negative outcomes in certain extreme cases. Therefore, when proposing and implementing such policies, a thorough examination of the specific circumstances is highly recommended to avoid any unintended consequences.

4 Conclusions

We have presented a highly flexible and powerful conditional generative framework, designed to capture the counterfactual distribution of outcomes when treatments vary over time. Statistically, our framework has approximated the true counterfactual distribution by minimizing the KL-divergence between the model distribution and the proxy conditional distribution represented by a conditional generator. We have demonstrated that our framework has competitive performance over state-of-the-art baselines in synthetic settings and yields compelling results in a real data set on COVID-19 mask mandate. Our work has facilitated the synergy between generative models and causal inference in time series settings.

References

- [1] Dhaval Adjudah, Karthik Dinakar, Matteo Chinazzi, Samuel P Fraiberger, Alex Pentland, Samantha Bates, Kyle Staller, Alessandro Vespignani, and Deepak L Bhatt. Association between covid-19 outcomes and mask mandates, adherence, and attitudes. *PLoS One*, 16(6):e0252315, 2021.

- [2] Ahmed M Alaa and Mihaela Van Der Schaar. Bayesian inference of individualized treatment effects using multi-task gaussian processes. *Advances in neural information processing systems*, 30, 2017.
- [3] Vahid Balazadeh Meresht, Vasilis Syrgkanis, and Rahul G Krishnan. Partial identification of treatment effects with implicit generative models. *Advances in Neural Information Processing Systems*, 35:22816–22829, 2022.
- [4] Ioana Bica, Ahmed M Alaa, James Jordon, and Mihaela van der Schaar. Estimating counterfactual treatment outcomes over time through adversarially balanced representations. *arXiv preprint arXiv:2002.04083*, 2020.
- [5] U.S. Census Bureau. State population totals: 2020-2022. <https://www.census.gov/data/tables/time-series/demo/popest/2020s-state-total.html>. Accessed: 2022-09-15.
- [6] Yehu Chen, Annamaria Prati, Jacob Montgomery, and Roman Garnett. A multi-task gaussian process model for inferring time-varying treatment effects in panel data. In *International Conference on Artificial Intelligence and Statistics*, pages 4068–4088. PMLR, 2023.
- [7] Victor Chernozhukov, Iván Fernández-Val, and Blaise Melly. Inference on counterfactual distributions. *Econometrica*, 81(6):2205–2268, 2013.
- [8] John DiNardo, Nicole M. Fortin, and Thomas Lemieux. Labor market institutions and the distribution of wages, 1973-1992: A semiparametric approach. *Econometrica*, 64(5):1001–1044, 1996.
- [9] Garrett Fitzmaurice, Marie Davidian, Geert Verbeke, and Geert Molenberghs. *Longitudinal data analysis*. CRC press, 2008.
- [10] Centers for Disease Control, Prevention, et al. Us state and territorial public mask mandates from april 10, 2020 through august 15, 2021 by county by day. *Policy Surveillance. September*, 10, 2021.
- [11] Charlie Frogner, Chiyuan Zhang, Hossein Mobahi, Mauricio Araya, and Tomaso A Poggio. Learning with a wasserstein loss. *Advances in neural information processing systems*, 28, 2015.
- [12] Keisuke Fujii, Koh Takeuchi, Atsushi Kuribayashi, Naoya Takeishi, Yoshinobu Kawahara, and Kazuya Takeda. Estimating counterfactual treatment outcomes over time in complex multi-agent scenarios. *arXiv preprint arXiv:2206.01900*, 2022.
- [13] Google. Community mobility reports. <https://www.google.com/covid19/mobility/>, 2022. Accessed: 2022-09-15.
- [14] Olivier Goudet, Diviyani Kalainathan, Philippe Caillou, Isabelle Guyon, David Lopez-Paz, and Michèle Sebag. Causal generative neural networks. *arXiv preprint arXiv:1711.08936*, 2017.
- [15] CMU DELPHI Group. Covid-19 symptom surveys through facebook. <https://delphi.cmu.edu/blog/2020/08/26/covid-19-symptom-surveys-through-facebook/>. Accessed: 2022-09-15.

- [16] Gery P Guy Jr, Florence C Lee, Gregory Sunshine, Russell McCord, Mara Howard-Williams, Lyudmyla Kompaniyets, Christopher Dunphy, Maxim Gakh, Regen Weber, Erin Sauber-Schatz, et al. Association of state-issued mask mandates and allowing on-premises restaurant dining with county-level covid-19 case and death growth rates—united states, march 1–december 31, 2020. *Morbidity and Mortality Weekly Report*, 70(10):350, 2021.
- [17] Keisuke Hirano, Guido W Imbens, and Geert Ridder. Efficient estimation of average treatment effects using the estimated propensity score. *Econometrica*, 71(4):1161–1189, 2003.
- [18] Jonathan Ho, Ajay Jain, and Pieter Abbeel. Denoising diffusion probabilistic models. *Advances in Neural Information Processing Systems*, 33:6840–6851, 2020.
- [19] Daniel Jiwoong Im, Kyunghyun Cho, and Narges Razavian. Causal effect variational autoencoder with uniform treatment. *arXiv preprint arXiv:2111.08656*, 2021.
- [20] Kosuke Imai and David A Van Dyk. Causal inference with general treatment regimes: Generalizing the propensity score. *Journal of the American Statistical Association*, 99(467):854–866, 2004.
- [21] Guido W Imbens. Nonparametric estimation of average treatment effects under exogeneity: A review. *Review of Economics and statistics*, 86(1):4–29, 2004.
- [22] Edward H Kennedy, Sivaraman Balakrishnan, and Larry Wasserman. Semiparametric counterfactual density estimation. *arXiv preprint arXiv:2102.12034*, 2021.
- [23] Diederik Kingma, Tim Salimans, Ben Poole, and Jonathan Ho. Variational diffusion models. *Advances in neural information processing systems*, 34:21696–21707, 2021.
- [24] Diederik P Kingma and Jimmy Ba. Adam: A method for stochastic optimization. *arXiv preprint arXiv:1412.6980*, 2014.
- [25] Diederik P Kingma and Max Welling. Auto-encoding variational bayes. *arXiv preprint arXiv:1312.6114*, 2013.
- [26] Diederik P Kingma, Max Welling, et al. An introduction to variational autoencoders. *Foundations and Trends® in Machine Learning*, 12(4):307–392, 2019.
- [27] Samantha Kleinberg and George Hripcsak. A review of causal inference for biomedical informatics. *Journal of biomedical informatics*, 44(6):1102–1112, 2011.
- [28] Milan Kuzmanovic, Tobias Hatt, and Stefan Feuerriegel. Deconfounding temporal autoencoder: estimating treatment effects over time using noisy proxies. In *Machine Learning for Health*, pages 143–155. PMLR, 2021.
- [29] Bryan Lim. Forecasting treatment responses over time using recurrent marginal structural networks. *Advances in neural information processing systems*, 31, 2018.
- [30] Jaechang Lim, Seongok Ryu, Jin Woo Kim, and Woo Youn Kim. Molecular generative model based on conditional variational autoencoder for de novo molecular design. *Journal of cheminformatics*, 10(1):1–9, 2018.
- [31] Qiao Liu, Zhongren Chen, and Wing Hung Wong. Causalegm: a general causal inference framework by encoding generative modeling. *arXiv preprint arXiv:2212.05925*, 2022.

- [32] Christos Louizos, Uri Shalit, Joris M Mooij, David Sontag, Richard Zemel, and Max Welling. Causal effect inference with deep latent-variable models. *Advances in neural information processing systems*, 30, 2017.
- [33] Helena C Maltezou, Androula Pavli, and Athanasios Tsakris. Post-covid syndrome: an insight on its pathogenesis. *Vaccines*, 9(5):497, 2021.
- [34] Mehdi Mirza and Simon Osindero. Conditional generative adversarial nets, 2014. cite arxiv:1411.1784.
- [35] Ashish Mishra, Shiva Krishna Reddy, Anurag Mittal, and Hema A Murthy. A generative model for zero shot learning using conditional variational autoencoders. In *Proceedings of the IEEE conference on computer vision and pattern recognition workshops*, pages 2188–2196, 2018.
- [36] Kevin P Murphy. *Machine learning: a probabilistic perspective*. MIT press, 2012.
- [37] Jersey Neyman. Sur les applications de la théorie des probabilités aux expériences agricoles: Essai des principes. *Roczniki Nauk Rolniczych*, 10(1):1–51, 1923.
- [38] My Nguyen. Mask mandates and covid-19 related symptoms in the us. *ClinicoEconomics and Outcomes Research*, pages 757–766, 2021.
- [39] Artidoro Pagnoni, Kevin Liu, and Shangyan Li. Conditional variational autoencoder for neural machine translation. *arXiv preprint arXiv:1812.04405*, 2018.
- [40] Victor M Panaretos and Yoav Zemel. Statistical aspects of wasserstein distances. *Annual review of statistics and its application*, 6:405–431, 2019.
- [41] Judea Pearl. Causal inference in statistics: An overview. 2009.
- [42] Hadrien Reynaud, Athanasios Vlontzos, Mischa Dombrowski, Ciarán Gilligan Lee, Arian Beqiri, Paul Leeson, and Bernhard Kainz. D’artagnan: Counterfactual video generation. In *Medical Image Computing and Computer Assisted Intervention–MICCAI 2022: 25th International Conference, Singapore, September 18–22, 2022, Proceedings, Part VIII*, pages 599–609. Springer, 2022.
- [43] James Robins. A new approach to causal inference in mortality studies with a sustained exposure period—application to control of the healthy worker survivor effect. *Mathematical modelling*, 7(9-12):1393–1512, 1986.
- [44] James M Robins. Correcting for non-compliance in randomized trials using structural nested mean models. *Communications in Statistics-Theory and methods*, 23(8):2379–2412, 1994.
- [45] James M Robins. Association, causation, and marginal structural models. *Synthese*, 121(1/2):151–179, 1999.
- [46] James M Robins, Sander Greenland, and Fu-Chang Hu. Estimation of the causal effect of a time-varying exposure on the marginal mean of a repeated binary outcome. *Journal of the American Statistical Association*, 94(447):687–700, 1999.
- [47] James M Robins, Miguel Angel Hernan, and Babette Brumback. Marginal structural models and causal inference in epidemiology. *Epidemiology*, pages 550–560, 2000.

- [48] James M Robins, Andrea Rotnitzky, and Lue Ping Zhao. Estimation of regression coefficients when some regressors are not always observed. *Journal of the American statistical Association*, 89(427):846–866, 1994.
- [49] Paul R Rosenbaum and Donald B Rubin. The central role of the propensity score in observational studies for causal effects. *Biometrika*, 70(1):41–55, 1983.
- [50] Murray Rosenblatt. Remarks on some nonparametric estimates of a density function. *The annals of mathematical statistics*, pages 832–837, 1956.
- [51] Donald B Rubin. Bayesian inference for causal effects: The role of randomization. *The Annals of statistics*, pages 34–58, 1978.
- [52] Shiv Kumar Saini, Sunny Dhamnani, Akil Arif Ibrahim, and Prithviraj Chavan. Multiple treatment effect estimation using deep generative model with task embedding. In *The World Wide Web Conference*, pages 1601–1611, 2019.
- [53] Axel Sauer and Andreas Geiger. Counterfactual generative networks. *arXiv preprint arXiv:2101.06046*, 2021.
- [54] Peter Schulam and Suchi Saria. Reliable decision support using counterfactual models. *Advances in neural information processing systems*, 30, 2017.
- [55] Nabeel Seedat, Fergus Imrie, Alexis Bellot, Zhaozhi Qian, and Mihaela van der Schaar. Continuous-time modeling of counterfactual outcomes using neural controlled differential equations. *arXiv preprint arXiv:2206.08311*, 2022.
- [56] Jascha Sohl-Dickstein, Eric Weiss, Niru Maheswaranathan, and Surya Ganguli. Deep unsupervised learning using nonequilibrium thermodynamics. In Francis Bach and David Blei, editors, *Proceedings of the 32nd International Conference on Machine Learning*, volume 37 of *Proceedings of Machine Learning Research*, pages 2256–2265, Lille, France, 07–09 Jul 2015. PMLR.
- [57] Kihyuk Sohn, Honglak Lee, and Xinchen Yan. Learning structured output representation using deep conditional generative models. *Advances in neural information processing systems*, 28, 2015.
- [58] The New York Times. Coronavirus (covid-19) data in the united states. <https://github.com/nytimes/covid-19-data>, 2021. Accessed: 2022-09-15.
- [59] SS Vallender. Calculation of the wasserstein distance between probability distributions on the line. *Theory of Probability & Its Applications*, 18(4):784–786, 1974.
- [60] Miriam E Van Dyke, Tia M Rogers, Eric Pevzner, Catherine L Satterwhite, Hina B Shah, Wyatt J Beckman, Farah Ahmed, D Charles Hunt, and John Rule. Trends in county-level covid-19 incidence in counties with and without a mask mandate—kansas, june 1–august 23, 2020. *Morbidity and Mortality Weekly Report*, 69(47):1777, 2020.
- [61] Arnaud Van Looveren, Janis Klaise, Giovanni Vacanti, and Oliver Cobb. Conditional generative models for counterfactual explanations. *arXiv preprint arXiv:2101.10123*, 2021.
- [62] Lan Wang, Yu Zhou, Rui Song, and Ben Sherwood. Quantile-optimal treatment regimes. *Journal of the American Statistical Association*, 113(523):1243–1254, 2018.
- [63] Yuxin Wang, Zicheng Deng, and Donglu Shi. How effective is a mask in preventing covid-19 infection? *Medical devices & sensors*, 4(1):e10163, 2021.

- [64] Yongling Xiao, Michal Abrahamowicz, and Erica EM Moodie. Accuracy of conventional and marginal structural cox model estimators: a simulation study. *The international journal of biostatistics*, 6(2), 2010.
- [65] Jinsung Yoon, James Jordon, and Mihaela Van Der Schaar. Ganite: Estimation of individualized treatment effects using generative adversarial nets. In *International conference on learning representations*, 2018.
- [66] Weijia Zhang, Thuc Duy Le, Lin Liu, Zhi-Hua Zhou, and Jiuyong Li. Mining heterogeneous causal effects for personalized cancer treatment. *Bioinformatics*, 33(15):2372–2378, 2017.
- [67] YiFan Zhang, Hanlin Zhang, Zachary Chase Lipton, Li Erran Li, and Eric Xing. Exploring transformer backbones for heterogeneous treatment effect estimation. In *NeurIPS ML Safety Workshop*, 2022.
- [68] Shixiang Zhu, Alexander Bukharin, Liyan Xie, Mauricio Santillana, Shihao Yang, and Yao Xie. High-resolution spatio-temporal model for county-level covid-19 activity in the U.S. *ACM Trans. Manage. Inf. Syst.*, 12(4), sep 2021.
- [69] Shixiang Zhu, Alexander Bukharin, Liyan Xie, Khurram Yamin, Shihao Yang, Pinar Keskinocak, and Yao Xie. Early detection of COVID-19 hotspots using spatio-temporal data. *IEEE Journal of Selected Topics in Signal Processing*, 16(2):250–260, 2022.

A Assumptions

The standard assumptions needed for identifying the treatment effects are [9, 29, 54]:

1. *Consistency*: If $\bar{A}_t = \bar{a}_t$ for a given subject, then the counterfactual outcome for treatment, \bar{a}_t , is the same as the observed (factual) outcome: $Y(\bar{a}_t) = Y$.
2. *Positivity*: If $\mathbb{P}\{\bar{A}_{t-1} = \bar{a}_{t-1}, \bar{X}_t = \bar{x}_t\} \neq 0$, then $\mathbb{P}\{\bar{A}_t = \bar{a}_t | \bar{A}_{t-1} = \bar{a}_{t-1}, \bar{X}_t = \bar{x}_t\} > 0$ for all \bar{a}_t [20].
3. *Sequential strong ignorability*: $Y(\bar{a}_t) \perp\!\!\!\perp \bar{A}_t | \bar{A}_{t-1} = \bar{a}_{t-1}, \bar{X}_t = \bar{x}_t$, for all a_t and t .

Assumption 2 means that, for each timestep, each treatment has non-zero probability of being assigned. Assumption 3 (also called conditional exchangeability) means that there are no unmeasured confounders, that is, all of covariates affecting both the treatment assignment and the outcomes are present in the the observational data set. Note that while assumption 3 is standard across all methods for estimating treatment effects, it is not testable in practice [41, 47].

B Proof of Lemma 1

Given a probability distribution for (Y, \bar{A}, \bar{X}) and a causal directed acyclic graph (DAG) shown in Figure 6, we can factor $f(Y, \bar{A}, \bar{X})$ as

$$f(Y, \bar{A}, \bar{X}) = f(y | \bar{A}, \bar{X}) \prod_{\tau=t-d}^t f(X_\tau | \bar{A}_{\tau-1}, \bar{X}_{\tau-1}) \prod_{\tau=t-d}^t f(A_\tau | \bar{A}_{\tau-1}, \bar{X}_\tau). \quad (7)$$

Using g-formula [45], we have

$$\begin{aligned} f_{\bar{a}}(y) &= \int f(y | \bar{a}, \bar{X}) \cdot \prod_{\tau=t-d}^t f(X_\tau | \bar{a}_{\tau-1}, \bar{X}_{\tau-1}) d\bar{X} \\ &= \int f(y | \bar{a}, \bar{X}) \cdot \frac{\prod_{\tau=t-d}^t f(a_\tau | \bar{a}_{\tau-1}, \bar{X}_\tau)}{\prod_{\tau=t-d}^t f(a_\tau | \bar{a}_{\tau-1}, \bar{X}_\tau)} \cdot \prod_{\tau=t-d}^t f(X_\tau | \bar{a}_{\tau-1}, \bar{X}_{\tau-1}) d\bar{X} \\ &\stackrel{(i)}{=} \int \frac{1}{\prod_{\tau=t-d}^t f(a_\tau | \bar{a}_{\tau-1}, \bar{X}_\tau)} f(y, \bar{a}, \bar{X}) d\bar{X} \\ &= \int \frac{\mathbb{1}\{\bar{A} = \bar{a}\}}{\prod_{\tau=t-d}^t f(A_\tau | \bar{A}_{\tau-1}, \bar{X}_\tau)} f(y, \bar{A}, \bar{X}) d\bar{A} d\bar{X}, \end{aligned}$$

where the equation (i) holds due to (7).

C Proof of Proposition 1

Note that the unstabilized weight is defined as $w(\bar{A}, \bar{X}) = 1 / \prod_{\tau=t-d}^t f(A_\tau | \bar{A}_{\tau-1}, \bar{X}_\tau)$. Using Lemma 1, we have

$$\begin{aligned} \mathbb{E}_{y \sim f_{\bar{a}}} \log f_\theta(y | \bar{a}) &= \int \log f_\theta(y | \bar{a}) f_{\bar{a}}(y) dy \\ &= \int \log f_\theta(y | \bar{a}) \int \frac{\mathbb{1}\{\bar{A} = \bar{a}\}}{\prod_{\tau=t-d}^t f(A_\tau | \bar{A}_{\tau-1}, \bar{X}_\tau)} f(y, \bar{A}, \bar{X}) d\bar{A} d\bar{X} dy \end{aligned}$$

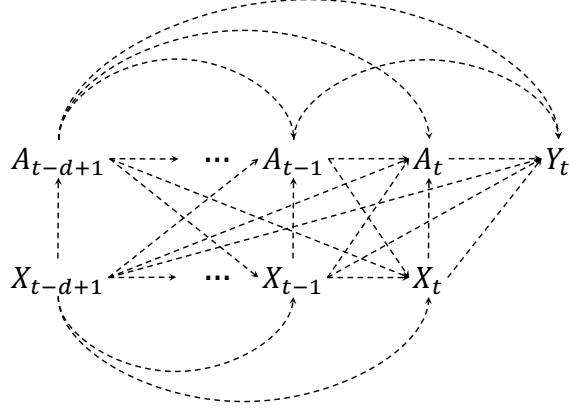


Figure 6: The causal directed acyclic graph (DAG) of the time-varying treatment.

$$\begin{aligned}
&= \int \log f_\theta(y|\bar{a}) \int w(\bar{A}, \bar{X}) \mathbb{1}\{\bar{A} = \bar{a}\} f(y, \bar{A}, \bar{X}) d\bar{A} d\bar{X} dy \\
&= \int \log f_\theta(y|\bar{a}) \int w(\bar{a}, \bar{X}) f(y, \bar{a}, \bar{X}) d\bar{X} dy \\
&= \int \int \log f_\theta(y|\bar{a}) w(\bar{a}, \bar{X}) f(y, \bar{a}, \bar{X}) d\bar{X} dy \\
&= \int \int \log f_\theta(y|\bar{a}) w(\bar{a}, \bar{X}) f(y, \bar{a}|\bar{X}) f(\bar{X}) dy d\bar{X} \\
&\stackrel{(i)}{=} \int w(\bar{a}, \bar{X}) f(\bar{X}) \mathbb{E}_{(y, \bar{a})} [\log f_\theta(y|\bar{a})|\bar{X}] d\bar{X} \\
&= \mathbb{E}_{\bar{X}} \left[\mathbb{E}_{(y, \bar{a})} [w(\bar{a}, \bar{X}) \log f_\theta(y|\bar{a})|\bar{X}] \right] \\
&\stackrel{(ii)}{=} \mathbb{E}_{(y, \bar{a}, \bar{x}) \sim f} w(\bar{a}, \bar{x}) \log f_\theta(y|\bar{a}) \\
&\approx \sum_{(y, \bar{a}, \bar{x}) \in \mathcal{D}} w(\bar{a}, \bar{x}) \log f_\theta(y|\bar{a}),
\end{aligned}$$

where (i) follows from Fubini's theorem and (ii) follows from the tower property of expectation.

D Derivation and implementation details of variational learning

Derivation of the proxy conditional distribution Now we present the derivation of the log conditional probability density function (PDF) in (6). To begin with, it can be written as:

$$\log f_\theta(y|\bar{a}) = \log \int p_\theta(y, z|\bar{a}) dz,$$

where z is a latent random variable. This integral has no closed form and can be usually estimated by Monte Carlo integration with importance sampling, *i.e.*,

$$\int p_\theta(y, z|\bar{a}) dz = \mathbb{E}_{z \sim q(\cdot|y, \bar{a})} \left[\frac{p_\theta(y, z|\bar{a})}{q(z|y, \bar{a})} \right].$$

Here $q(z|y, \bar{a})$ is the proposed variational distribution, where we can draw sample z from this distribution given y and \bar{a} . Therefore, by Jensen's inequality, we can find the evidence lower

bound (ELBO) of the conditional PDF:

$$\log f_\theta(y|\bar{a}) = \log \mathbb{E}_{z \sim q(\cdot|y,\bar{a})} \left[\frac{p_\theta(y, z|\bar{a})}{q(z|y, \bar{a})} \right] \geq \mathbb{E}_{z \sim q(\cdot|y,\bar{a})} \left[\log \frac{p_\theta(y, z|\bar{a})}{q(z|y, \bar{a})} \right].$$

Using Bayes rule, the ELBO can be equivalently expressed as:

$$\begin{aligned} \mathbb{E}_{z \sim q(\cdot|y,\bar{a})} \left[\log \frac{p_\theta(y, z|\bar{a})}{q(z|y, \bar{a})} \right] &= \mathbb{E}_{z \sim q(\cdot|y,\bar{a})} \left[\log \frac{p_\theta(y|z, \bar{a})p_\theta(z|\bar{a})}{q(z|y, \bar{a})} \right] \\ &= \mathbb{E}_{z \sim q(\cdot|y,\bar{a})} \left[\log \frac{p_\theta(z|\bar{a})}{q(z|y, \bar{a})} \right] + \mathbb{E}_{z \sim q(\cdot|y,\bar{a})} [\log p_\theta(y|z, \bar{a})] \\ &= -D_{\text{KL}}(q(z|y, \bar{a})||p_\theta(z|\bar{a})) + \mathbb{E}_{z \sim q(\cdot|y,\bar{a})} [\log p_\theta(y|z, \bar{a})]. \end{aligned}$$

Implementation details We parameterize both $p_\theta(z|\bar{a})$ and $q(z|y, \bar{a})$ using deep neural networks, denoted by g_{prior} and g_{encode} , respectively. A common choice is a simple factorized Gaussian encoder. For example, the approximate posterior $q(z|y, \bar{a})$ can be represented as:

$$q(z|y, \bar{a}) = \mathcal{N}(z; \mu, \text{diag}(\Sigma)),$$

or

$$q(z|y, \bar{a}) = \prod_{j=1}^r q(z_j|y, \bar{a}) = \prod_{j=1}^r \mathcal{N}(z_j; \mu_j, \sigma_j^2).$$

The Gaussian parameters $\mu = (\mu_j)_{j=1, \dots, r}$ and $\text{diag}(\Sigma) = (\sigma_j^2)_{j=1, \dots, r}$ can be obtained using reparameterization trick via an encoder network ϕ :

$$\begin{aligned} (\mu, \log \text{diag}(\Sigma)) &= \phi(y, \bar{a}), \\ z &= \mu + \sigma \odot \epsilon, \end{aligned}$$

where $\epsilon \sim \mathcal{N}(0, I)$ is another random variable and \odot is the element-wise product. For simplicity in presentation, we denote such a factorized Gaussian encoder as $g_{\text{encode}}(\epsilon, y, \bar{a})$ that maps an event y , its history \bar{a} , and a random noise vector ϵ to a sample from the approximate posterior for that event z .

In (6), the first term is the KL divergence of the approximate posterior from the prior, which acts as a regularizer, while the second term is an expected negative reconstruction error. They can be calculated as follows: (1) Because both $q(z|y_i, \bar{a}_{i-1})$ and $p_\theta(z|\bar{a}_{i-1})$ are modeled as Gaussian distributions, the KL divergence can be computed using a closed-form expression. (2) Maximizing the negative log-likelihood $p_\theta(y|z, \bar{a})$ is equivalent to minimizing the cross entropy between the distribution of an observed outcome y and the reconstructed outcome \tilde{y} generated by the generative model g given z and the history \bar{a} .

E Additional experiment details

E.1 Baselines

Here we present an additional review of each baseline method in the paper as well as implementation details.

Linear marginal structural model (MSM) We include the classic MSM proposed in [48, 43]. This model assumes that the counterfactual mean of the outcome variable can be represented as a linear function of the treatments. We use this model as a means to validate the marginal dependence of the outcome on the treatment. It serves as a sanity check to ensure that the relationship between the treatment and the outcome aligns with our expectations. We learn the MSM using stochastic gradient descent with a weighted loss function:

$$\sum_{(y, \bar{a}, \bar{x}) \in \mathcal{D}} w_{\phi}(\bar{a}, \bar{x})(y - g_{\text{msm}}(\bar{a}))^2,$$

where g_{msm} is the linear MSM. To establish a fair comparison, we train the MSM using an identical training size to that of the MSCVAE model. We train the MSM for 1,000 epochs with a learning rate of 0.1. However, it’s important to note that in this particular setup, our capacity is limited to estimating the mean instead of the entire distribution. Consequently, we only calculate the mean distance metric for this baseline model.

Conditional variational autoencoder (CVAE) To examine the impact of Inverse Probability of Treatment Weighting (IPTW) on training generative models, we include a vanilla conditional variational autoencoder (CVAE) with an architecture identical to that of the MSCVAE, but excluding IPTW weighting. The CVAE is a widely-used type of conditional generative model that has found applications in various tasks, including image generation [35, 57], neural machine translation [39], and molecular design [30]. To train the CVAE, we follow the same procedure as MSCVAE, with the exception that we replace the loss function with the unweighted version of (4).

$$\sum_{(y, \bar{a}, \bar{x}) \in \mathcal{D}} \log f_{\theta}(y|\bar{a}),$$

where $f_{\theta}(\cdot)$ is the conditional distribution represented by the CVAE.

Kernel density estimator (KDE) We use a Gaussian kernel density estimator [50] to estimate the empirical distribution from the observed data. This is achieved by running KDE on the observed outcomes with the same treatments, *i.e.*,

$$f_{\bar{a}} \approx g_{\text{kde}}(y|\bar{A} = \bar{a}),$$

where $g_{\text{kde}}(\cdot)$ is the KDE estimator. We learn the KDE with bandwidth set to 0.5, 1, 1.5, and 2, respectively, and report the metrics with bandwidth = 0.5 as the optimal results.

Kernel density estimator based on IPTW (IPTW+KDE) We also use a Gaussian kernel density estimator to estimate the empirical distribution from the reweighted pseudo population. This is achieved by running KDE on $y|\bar{A} = \bar{a}$ where each sample tuple (y, \bar{a}, \bar{x}) is weighted by its IPTW, $w_{\phi}(\bar{a}, \bar{x})$. The bandwidth is set to be the same as in KDE.

E.2 Experiment set-up

The counterfactual generator g_{θ} , the IPTW w_{ϕ} , and the encoder network g_{encode} share the same two-layer fully-connected network architecture with ReLU activation. The layer width is set to 1,000, and the length of the latent variable z is set to h which is determined by the specific synthetic experiment setting: $h = 5$ for $d = 1$ and $d = 3$, $h = 10$ for $d = 5$ and the real data. For g_{encode} , the fully-connected networks map the $d + 1$ dimensional input vector (consisting of a d -dimensional treatment and 1-dimensional response) to the h -dimensional latent representation.

Table 2: Coefficients of the linear model in synthetic data generation

	α	β	γ
$d = 1$	(-3, 2, -1)	(-0.5, 0.5, 0.5, -0.5)	(0, 1, -1)
$d = 3$	(-1, 12, 6, 3, 2, 1, 0.5)	(-0.5, 0.5, -0.5, 0.5, 0.5, -0.5, 0.5, -0.5)	(-1, 1.5, 1, 0.5, -1.5, -1, -0.5)
$d = 5$	(-1, 12, 6, 3, 1, 0.5, 2, 1, 0.5, 0.1, 0.05)	(-0.5, 0.5, -0.5, 0.5, -0.5, 0.5, 0.5, -0.5, 0.5, -0.5, 0.5, -0.5)	(-1, 1.5, 1, 0.5, 0.1, 0.05, -1.5, -1, -0.5, -0.1, -0.05)

For g_θ , the fully-connected networks map the $h + d$ dimensional input vector (consisting of a d -dimensional treatment and h -random noise) to the 1-dimensional generated counterfactual outcome. For w_ϕ , the fully-connected networks map the $2d$ -dimensional input vector (consisting of a d -dimensional treatment and d -dimensional covariate) to the 1-dimensional conditional probability. We use a Sigmoid output layer for w_ϕ to ensure the output falls within $[0, 1]$. We set the batch size to 256 and the number of training epochs to 200 for training all the models in both synthetic and real data setting. The learning rate was set to 10^{-3} with a linear step-wise learning rate scheduler (Pytorch learning rate scheduler function `StepLR`) to ensure stable convergence of the learning process.

E.3 Synthetic data

In this section, we provide an overview of the procedures for generating synthetic data. Our goal is to evaluate the performance of the proposed MSCVAE method and compare it to baseline approaches in the context of time-varying treatments. We follow the classic setting in [46] and simulate time series data with time-varying treatments and covariates. The presence of the time-varying confounders serves as an appropriate testbed for comparing MSM-based models to the baselines. To be specific, we generate three synthetic data sets with varying levels of historical dependence denoted as d . Each data set consists of 10,000 trajectories, which represent recorded observations of individual subjects. These trajectories comprise 100 data tuples, encompassing treatment, covariate, and outcome values at specific time points. The causal relationships between these variables are visually depicted in Figure 6. For each time trajectory of length T , the data sets are generated based on the following equations:

$$X_0 \sim \text{uniform}(0, 1), \quad (8)$$

$$X_t = \gamma_0 + \sum_{\tau=t-d}^{t-1} \gamma_{t-\tau} A_\tau + \sum_{\tau=t-d}^{t-1} \gamma_{d+t-\tau} X_\tau, \quad (9)$$

$$\mathbb{P}\{A_t = 1\} = \sigma\left(\beta_0 + \sum_{\tau=t-d}^{t-1} \beta_{t-\tau} A_\tau + \sum_{\tau=t-d}^t \beta_{d+t-\tau} X_\tau\right), \quad (10)$$

$$Y_t = \alpha_0 + \sum_{\tau=t-d}^{t-1} \alpha_{t-\tau} A_\tau + \sum_{\tau=t-d}^{t-1} \alpha_{d+t-\tau} X_\tau + \epsilon, \quad (11)$$

where $\epsilon \sim \mathcal{N}(0, 0.05)$ is the observation noise and $\sigma(\cdot)$ is a Sigmoid function. The specific coefficients are set according to the values in Table 2 to ensure the generation of valid synthetic data distributions with diversity:

In our experiments, we set $\beta_0 = -0.5$ for the balanced treatment combinations and $\beta_0 = -2$ for the imbalanced treatment combinations. The rationale behind adjusting β_0 is as follows: while keeping the remaining β coefficients, treatment variables \bar{a} , and covariates \bar{x} unchanged, a smaller value of β_0 reduces the probability of treatment exposure, *i.e.*, $\mathbb{P}(A_t = 1)$. Consequently, this lower probability of treatment exposure results in a decrease in the occurrence of treatment combinations with exposures, leading to an imbalanced ratio among different treatment combinations.

Algorithm 2 Algorithm for obtaining a counterfactual sample

Input: Generated trajectory of a single subject: $\{(Y_t, X_t, A_t)\}_{t=1, \dots, T}$.

Initialization: Given the treatment history $\bar{A}_T = \bar{a}$.

for $\tau = T - d + 1 : T$ **do**

1. Generate the covariate x_τ based on $\bar{A}_{\tau-1}$ and $\bar{X}_{\tau-1}$ according to (9).

2. Update the covariate $\bar{X}_\tau \leftarrow x_\tau$.

end for

Generate $Y(\bar{a})$ based on \bar{A}_T and \bar{X}_T according to (11).

return $Y(\bar{a})$

Table 3: Real data description

Name	Description	Min	Max	Mean	Median	Std
Y	county-wise incremental new cases count	0	1.15×10^{-1}	2×10^{-3}	1×10^{-3}	2.7×10^{-3}
A	state-wise mask mandate	0	1×10^0	5.35×10^{-1}	1×10^0	4.99×10^{-1}
$X^{(0)}$	county-wise incremental death cases count	0	3.12×10^{-3}	3×10^{-4}	0	9×10^{-5}
$X^{(1)}$	state-wise average retail and recreation	-5.45×10^1	2.23×10^1	-4.27×10^0	-3.33×10^0	6.16×10^0
$X^{(2)}$	state-wise symptom value	0	3.23×10^1	9.3×10^{-1}	8.1×10^{-1}	5.1×10^{-1}

To ensure the validity of our synthetic data generation process, we verify that the three assumptions outlined in Appendix A are satisfied. Assumptions 1 and 3 are naturally met because the ground truth model guarantees that the counterfactual outcome equals the observed outcome and that there are no unmeasured confounders. As for assumption 2, since the conditional probability of treatment is the Sigmoid function applied to a finite linear combination of historical treatments and covariates, it will always be positive.

Once the synthetic data is generated, we obtain counterfactual distributions to assess the performance of our proposed method. Specifically, we use the synthetic data to obtain samples from the counterfactual outcome distribution, $Y(\bar{a})$, for any given treatment combination \bar{a} . This is achieved by iteratively fixing the treatment sequence in the time series and generating the covariates and response variables according to equations (9) and (11) for each of the 10,000 trajectories. The detailed procedure for obtaining a single counterfactual outcome sample is summarized in Algorithm 2.

E.4 Real data

The real data used in this study comprises COVID-19-related demographic statistics collected from 3,219 counties across 56 states/affiliated regions of the United States. The data covers a time period from 2020 to 2021, spanning 49 weeks. We obtained the data from reputable sources including the U.S. Census Bureau [5], the Center for Disease Control and Prevention [10], Google [13], the CMU DELPHI group’s Facebook survey [15], and the New York Times [58]. In our implementation, we assume a time lag of $d = 3$ for our model.

In our analysis, we select the outcome variable Y as the county-wise incremental cases count, and the treatment variable A as the state-wise mask mandate indicator variable. A value of 0 indicates no mask mandate, while a value of 1 indicates the enforcement of a mask mandate. Notably, we observe a pattern in the data where mask mandates are typically implemented simultaneously across all counties within a state. This synchronization justifies the use of the state-wise mask mandate count as the treatment variable. As for the covariates X , we choose the county-wise incremental death count, the state-wise average retail and recreation metric (representing changes in mobility levels compared to a baseline, which can be negative), and the state-wise symptom value. We excludes 89 counties with zero incremental

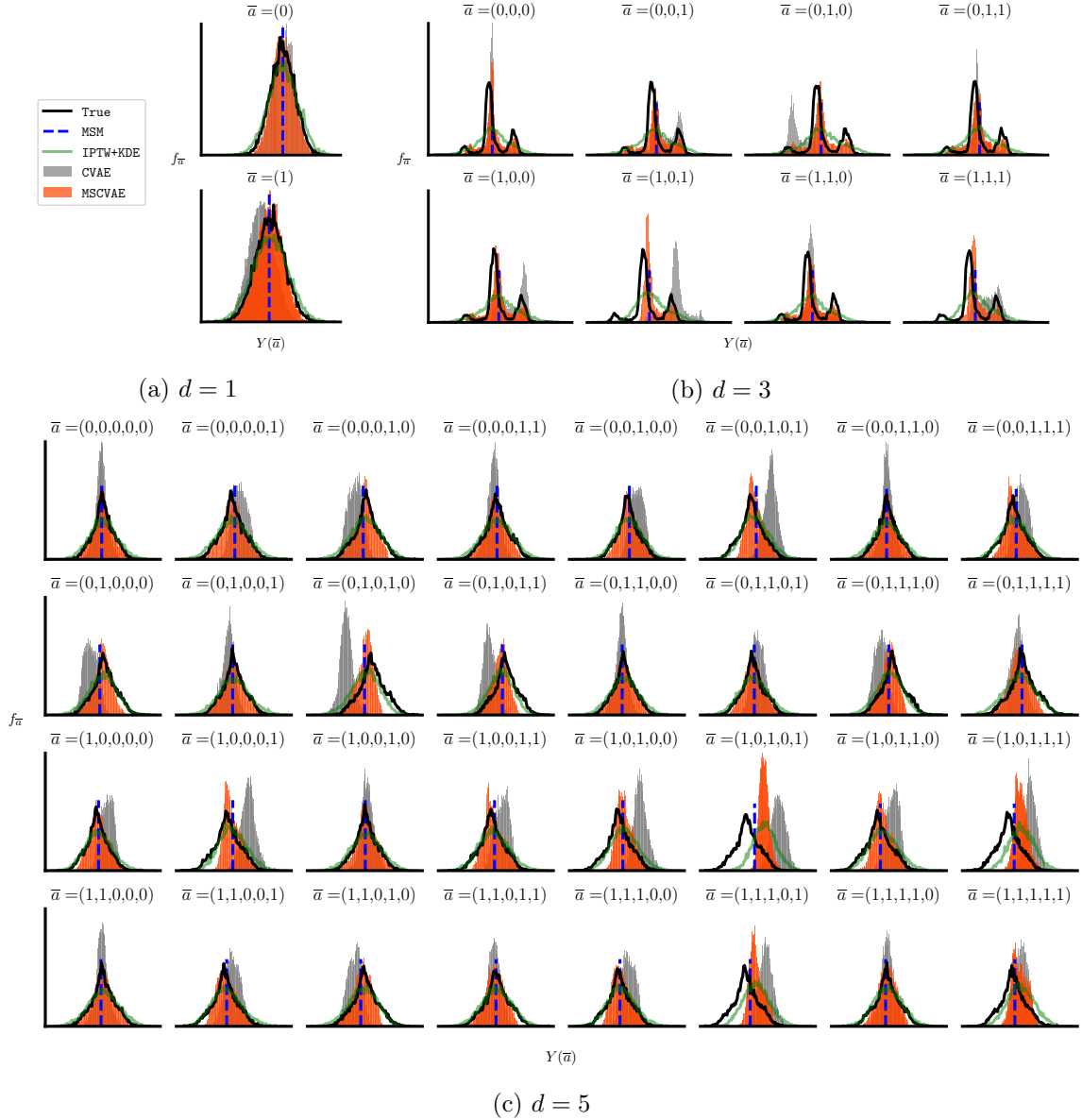


Figure 7: The estimated and true counterfactual distributions across various lengths of history dependence ($d = 1, 3, 5$) on synthetic data sets with imbalanced proportions of different treatment ($\beta_0 = -2$). Each sub-panel provides a comparison for a specific treatment combination \bar{a} .

new cases count. These counties either doesn't have significant amount of infectious cases or have small populations. To align the outcome variable with the covariates and treatment, we set it to measure one week after these variables. Due to the long-tailed distribution of the outcome variable, we apply a base-10 logarithmic transformation to enhance interpretability. Further details regarding the variables can be found in Table 3. We use the same model architecture described in Appendix E.2 to train the IPTW network and the MSCVAE. We generate counterfactual outcomes for treatment combinations $\bar{a} = (0, 0, 0)$ and $\bar{a} = (1, 1, 1)$. Since other treatment combinations occur rarely (less than 5% of observations), we exclude them from the final results.

F Additional synthetic results

In the main paper, we presented a visual comparison of the learned counterfactual distributions and the true counterfactual distribution for various scenarios ($d = 1, 3, 5$) with $\beta_0 = -0.5$, as shown in Figure 4. Here, in Figure 7, we provide a similar comparison with $\beta_0 = -2$, where the treatment combinations are an imbalanced distributed. Consistent with the findings in Figure 4, our results in Figure 7 demonstrate the superior performance of the MSCVAE model (represented by the orange shading) in accurately capturing the shape of the true counterfactual distributions (represented by the black line) across all scenarios. This observation further validates the quantitative comparisons presented in Table 1, where MSCVAE achieves the smallest mean and Wasserstein distance among all baseline methods. These results highlight that our algorithm attains competitive performance even when certain treatment combinations occur less frequently compared to others. This situation is common in real-life scenarios where certain treatment combinations are favored due to factors such as policy inertia.